

# Benzoyl Halide as Alternative Precursor for Synthesis of Lead Free Double Perovskite $\text{Cs}_3\text{Bi}_2\text{Br}_9$ Nanocrystals

Ashish Kumar<sup>1,2</sup>, S. S. Rawat<sup>1,2</sup>, Sanjay Kumar Swami<sup>1</sup>, Vidya Nand Singh<sup>1,2</sup>, and Ritu Srivastava<sup>1,\*</sup>

<sup>1</sup>CSIR-National Physical Laboratory, Dr. KS Krishnan Marg, New Delhi 110012, India

<sup>2</sup>Academy of Scientific and Innovative Research (AcSIR), Ghaziabad 201002, India

Ternary bismuth halides are interesting functional materials closely related to Pb halide perovskite photovoltaic material, and are widely sought after due to reduced toxicity of Bi compared to Pb. There are several reports on synthesis of  $\text{Cs}_3\text{Bi}_2\text{Br}_9$  nanocrystals (NCs) due to its being relatively stable compared to lead perovskite.  $\text{Cs}_3\text{Bi}_2\text{Br}_9$  nanocrystals have been synthesised using benzoyl bromide as an precursor using hot injection process at two different temperatures of 120 °C and 160 °C. Samples have been characterized for its structural, optical, microstructural and luminescent properties using X-ray diffraction, (XRD) UV-Vis spectroscopy, high resolution transmission electron microscopy and photoluminescent spectroscopy. XRD showed formation of  $\text{Cs}_3\text{Bi}_2\text{Br}_9$  phase with mono-crystalline structure. UV-Vis showed two types of band gap in the visible region which shows that the material can be used for photovoltaic applications. HRTEM confined the particles to be composed of nanocrystals with ~5 nm particles in the samples grown at 120 °C and it the particles joined together yield various structures composed of nanoparticles. The time resolved photoluminescence shows average life times of 3.067 ns and 4.761 ns for samples grown at two different temperatures. To the best of our knowledge, this is the first report where benzoyl halide has been used as alternative precursor for the synthesis of lead free double perovskite  $\text{Cs}_3\text{Bi}_2\text{Br}_9$  nanocrystals which have many applications.

**Keywords:** Double Perovskite, Nanocrystals, Photoluminescence and Quantum Yield.

## 1. INTRODUCTION

Organic and inorganic lead perovskite based materials have several optoelectronic applications. But the biggest issue with organic–inorganic lead based perovskites (LBP) are that they are very toxic and unstable under environmental conditions. Recently, several efforts have been made to grow lead free double perovskite (replacing Pb centre atom with Bi, Ag–Bi, Au, Ag–In, Sb, Ag–Sb etc.) and other lead free other perovskite materials (Pb replaced by  $\text{Cu}^{2+}$ ,  $\text{Sn}^{2+}$ ). Lately with focus on solving the stability as well as toxicity issue there was a report on organo-copper (environment friendly material) based perovskite materials. There are several reports on lead free double perovskite (elpasolite) based solar cell [1, 2]. The computational studies on double perovskite (elpasolites) have been carried out recently and growth of materials such as  $\text{Cs}_3\text{Bi}_2\text{X}_9$ ,  $\text{Cs}_2\text{AgBiX}_6$  (X = Cl, Br, I) and  $\text{Cs}_2\text{AgInCl}_6$  have been reported [3–4]. The lead based perovskite has

narrow emission and high photoluminescence quantum yield (PLQY) compared to lead free perovskite nanocrystals and quantum dots (QDs). In one of the report, lead ( $\text{Pb}^{2+}$ ) was replaced by less toxic Tin ( $\text{Sn}^{2+}$ ) atom as promising perovskite structure but tin based perovskite nanocrystals and QD shave low PLQE of about 0.14% and are very unstable. The Sn perovskite has 0.14% PLQE due to the presence of intrinsic defect sites and tin have two oxidation  $\text{Sn}^{2+}$  and  $\text{Sn}^{4+}$  [5]. The search for all inorganic cesium (Cs) based double perovskite which usually have less defect density compared with organic methyl ammonium based perovskite and better stability is continued. All-inorganic and air-stable  $\text{Cs}_3\text{Bi}_2\text{Br}_9$  perovskite nanocrystals show PLQY of only 0.2% when ligand free, shows PLQY of 4.5% when adding oleic acid (OA) is added. But bismuth halide based quantum dot show PLQE of 22% when treated with extra surfactant octylammonium bromide and oleic acid is added during the synthesis. The use of surfactant provides excellent thermal stability of more than 30 days and high luminescent properties.

\*Author to whom correspondence should be addressed.

This is because of passivation of surface trap-states and modification of intrinsic defect sites [6–9]. Cesium based inorganic perovskite under good stability as well as very less defect density compared with bulk organic–inorganic based perovskite (MA Based) [10–13]. All inorganic based perovskite has been reported that bismuth based bulk materials are highly crystalline nature with higher PLQE and better optoelectronics performance compared to MA based hybrid perovskite [14]. Therefore, in the present study, double perovskite  $\text{Cs}_3\text{Bi}_2\text{Br}_9$  nanocrystals having size in the range of 5–7 nm have been synthesized using the hot injection method and use of benzoyl halide as alternative precursor is an additional advantage. Benzoyl low cost material and easy to use for hot injection method directly injecting benzoyl bromide without any heating.

## 2. MATERIALS AND EXPERIMENTAL METHODS

### 2.1. Materials

Materials used for the synthesis with their sources are Bismuth neodecanoate (Sigma-Aldrich), Cesium acetate (99.9% Aldrich), Oleic acid (OA, 90%, Sigma-Aldrich), Oleylamine (Alfa Aesar), Octadecene (ODE), Toluene (Sigma), acetone (analytical pure) Ethyl Acetate (EA). Benzoyl Chloride, Lithium Bromide (LiBr). All materials were used as received without further purifications.

### 2.2. Synthesis of $\text{Cs}_3\text{Bi}_2\text{Br}_9$ Double Perovskite

1. Conversion of benzoyl chloride into benzoyl bromide: The reaction was performed in  $\text{N}_2$  atmosphere. 2 mL of benzoyl chloride was added to 1.7369 g of LiBr in 25 mL three neck flask. The flask was kept on a hot plate at 75 °C

for 4 h and the mixture was continuously stirred. The mixture converts from colourless to orange colour, indicating formation of benzoyl bromide. It was cooled down to room temperature (RT) and filtered using a PTFE membrane with 0.45  $\mu\text{m}$  pore size [15].

2.  $\text{Cs}(\text{OAc})$  (0.71 mmol), and bismuth neodecanoate (1 mmol) were dissolved in the combined mixture of octadecene (10 mL), oleic acid (2.8 mL) and oleylamine (1.9 mL). The reaction mixture was heated to 100 °C in vacuum for 90 min. After that reaction temperature was increased to 160 °C (sample 2) and 120 °C (samples 1) for 10 min in a nitrogen atmosphere. Neat 1 mL benzoyl bromide diluted with 1 mL ODE was swiftly injected. After 10 sec the reaction mixture was cooled down to room temperature in an ice-water bath. The yellow–green colloidal solution was obtained. Centrifugation of the reaction mixture was carried out to separate the yellow powder and supernatant. Yellow powder was dispersed into toluene and precipitated with acetone/EA and re-dispersed into toluene. The supernatant was purified by acetone/EA with dispersed a small amount of toluene for characterisation.

## 3. RESULTS AND DISCUSSION

### 3.1. XRD Characterisation

The previous report of  $\text{Cs}_3\text{Bi}_2\text{Br}_9$  single crystal was hexagonal structure with trigonal  $P3m1$  symmetry and crystal axis  $a = 0.796 \text{ nm} = b$  and  $c = 0.984 \text{ nm}$ . In the  $\text{Cs}_3\text{Bi}_2\text{Br}_9$  structure bismuth has body centred with  $\text{Cs}^+$  group is surrounded by six metal halide octahedral [16, 17]. The  $\text{Cs}_3\text{Bi}_2\text{Br}_9$  nanocrystal were synthesis by hot injection

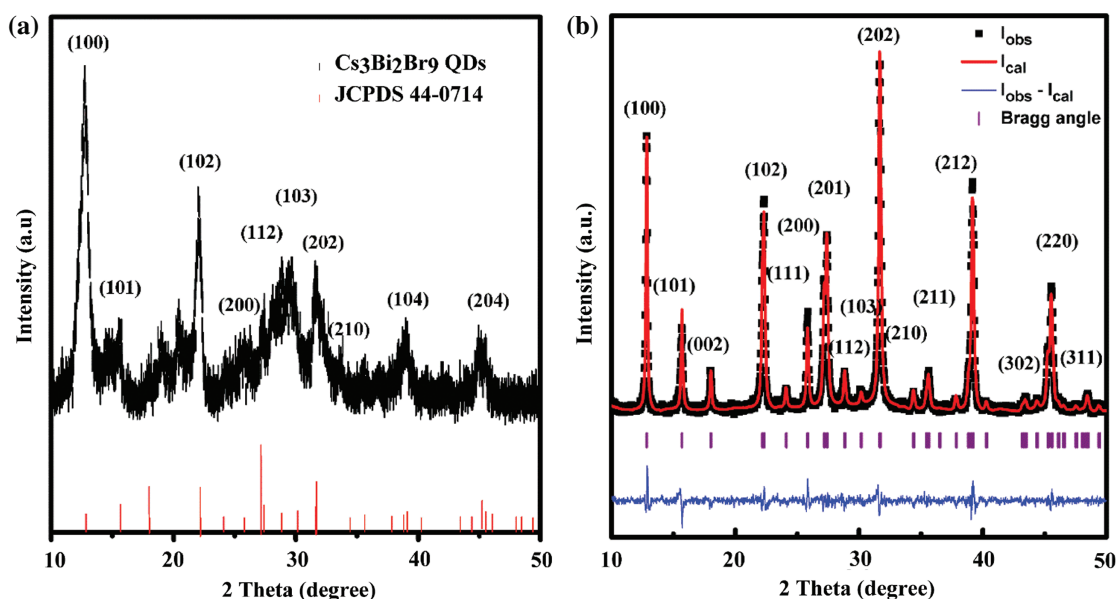


**Figure 1.** (a) XRD patterns of  $\text{Cs}_3\text{Bi}_2\text{Br}_9$  QDs with temperature 120 °C. (b) Result of the Rietveld refinement of XRD of  $\text{Cs}_3\text{Bi}_2\text{Br}_9$  NCs with data calculated curve position of allowed Bragg reflection with temperature 160 °C.

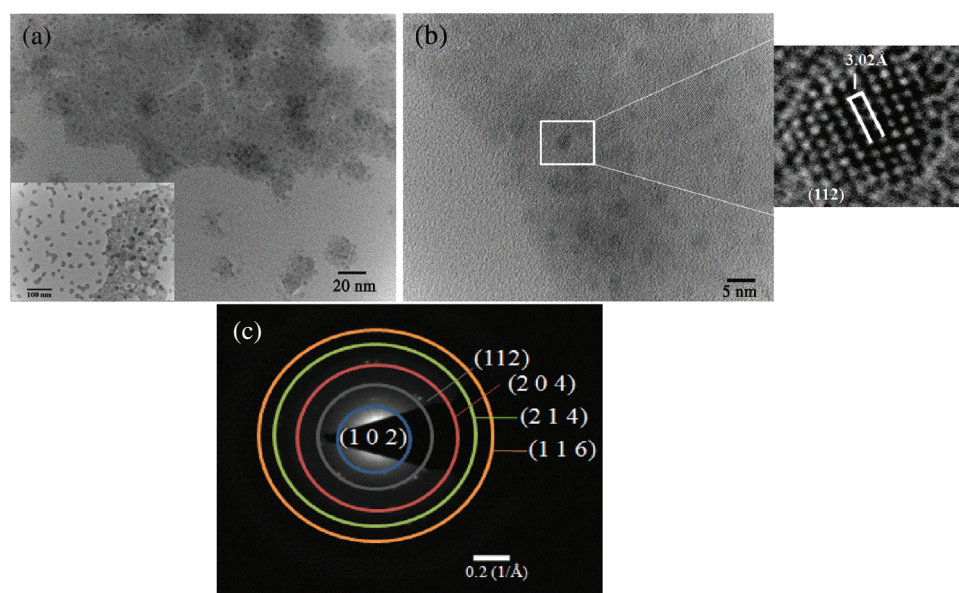


**Figure 2.** (a and b) Shows TEM, micrograph (c) shows SAED pattern and inset of figure (b) shows HRTEM lattice image of sample (1).

method. The yellow–green colloidal solution was obtained after purification with acetone wash. The ligand free yellow powder dispersed into toluene was used for XRD. For XRD characterisation film was made by drop casting the solution on glass substrate kept on hot plate in the glove box at a temperature of 100 °C. It was dried for 20 min. The results of XRD is shown in Figure 1(b) and analysis by Rietveld method is also shown. No other peaks except for  $\text{Cs}_3\text{Bi}_2\text{Br}_9$  is detected showing that the perovskite has

higher purity. The diffraction peaks are related to trigonal  $P3m1$  symmetry with space group 164 (JCPDS card no 44-0714) [18].

From Figure it is clear that the sample grown at 120 °C shows Nanocrystalline nature and the crystallinity has improved in the sample grown at 160 °C. The detailed analysis of XRD peaks shown in the supplementary information, it is clear that the peaks are shifted towards lower two theta value in the case of sample grown at 120 °C

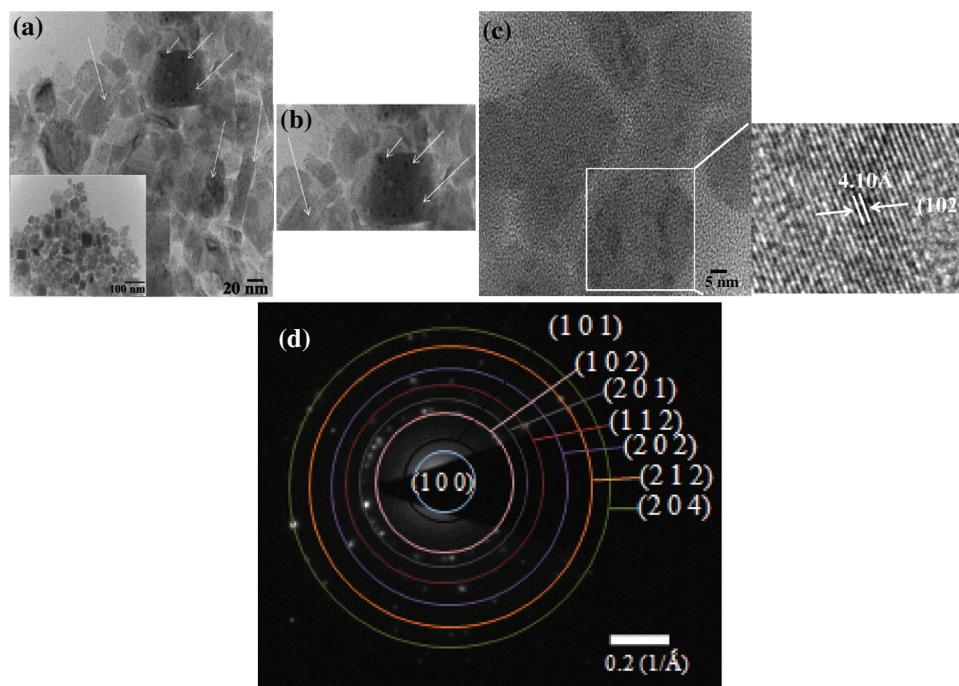


**Figure 3.** (a–c) Shows TEM, micrograph (d) shows SAED pattern and inset of figure (c) shows HRTEM lattice image of sample (2).

which indicates somewhat lattice expansion which is the case with the nanocrystalline materials. The peaks for sample grown at 160 °C shows very marginal shift which indicates that the sample is crystalline.

### 3.2. Transmission Electron Microscopy (TEM) Characterisation

Figures 2(a)–(b) show the Transmission Electron Microscopy (TEM) image of Cs<sub>3</sub>Bi<sub>2</sub>Br<sub>9</sub> (sample 1) QDs. The average size of spherical type particle is  $\sim 3.0 \pm .05$ . The high-resolution transmission electron microscopic (HRTEM) image is shown in the inset of Figure 2(b) shows the lattice spacing distance ( $d$ ) of 3.02 Å corresponding to the (112) crystal plane. The selective area electron diffraction (SAED) pattern shows polycrystalline nature of sample and planes are marked on the Figure 2(c). All the planes correspond to Cs<sub>3</sub>Bi<sub>2</sub>Br<sub>9</sub>.

Transmission Electron Microscopy (TEM) image of Cs<sub>3</sub>Bi<sub>2</sub>Br<sub>9</sub> (sample 2) nanocrystal is shown in Figures 3(a)–(b). The average size of tetragonal type particle is in the range of 10 to 70 nm. These tetragonal structures are made of 2 to 5 nm range spherical particle. The high-resolution transmission electron microscope (HRTEM) shown in inset of Figure 3(c) shows the lattice spacing distance ( $d$ ) of 4.10 Å corresponding to the (102) crystal plane. The SAED pattern shown in Figure 3(d) shows polycrystalline nature of the Cs<sub>3</sub>Bi<sub>2</sub>Br<sub>9</sub> nanocrystal and the planes are marked in the Figure 3(c).

From the TEM studies, it is clear that at 120 °C small particle are formed. When sample is made at 160 °C these particles coalesce and tetragonal structure is formed. The different temperature have different shaped structure [19].

### 3.3. UV-Vis and Photoluminescence (PL)

The UV-Vis absorption spectrum of Cs<sub>3</sub>Bi<sub>2</sub>Br<sub>9</sub> QDs is shown in Figure 4(a). In the spectrum a band edge exciton peak at 431 nm with tail up to 463 nm has been observed. In the case of single crystal and thin film the exciton peak were observed 459 and 440 nm. Thus, the exciton peak of sample 1 got blue shifted by 28 and 9 nm compared to single crystal and thin film values, respectively as the absorption spectrum depend upon growth temperature, exciton binding energy and quantum confinement effect [20]. The PL spectroscopy is one of the very important techniques to measure radiative recombination which can be used for photovoltaic application [21]. PL in lead free perovskite Cs<sub>3</sub>Bi<sub>2</sub>X<sub>9</sub> (X = Cl, Br, I) with PL emission wavelength ranging from 400 to 500 nm has been reported [22]. The ligand free Cs<sub>3</sub>Bi<sub>2</sub>Br<sub>9</sub> perovskite shows blue emission at 461 nm with FWHM (Full width Half Maximum) of 50.53 nm. Ligands free double perovskite does not show good PLQE as PL emission mostly arises from transition between valance band to conduction band through the fast trapping process. Although the raw data shows single PL peak at 461 nm with FWHM 50.53 nm

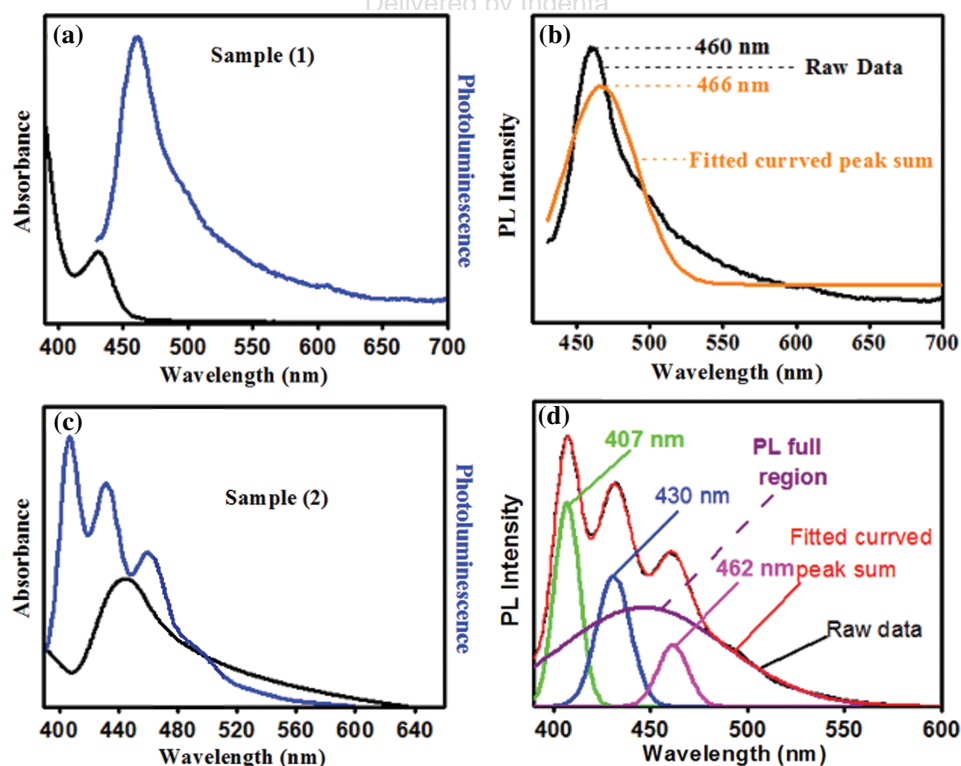


**Figure 4.** For sample 1 (a), UV-Vis and photoluminescence (PL). (b) PL fitting dat. For sample 2 (c), UV-Vis and photoluminescence (PL). (d) PL fitting dat.

the fitted PL data shows red shifted peak at 466 nm with FWHM 57 nm as shown in Figure 4(b).

The room temperature UV-Vis absorption spectrum of Cs<sub>3</sub>Bi<sub>2</sub>Br<sub>9</sub> perovskite NCs are shown in Figure 4(c). The broad absorption peak are illustrated in the absorption started approximately 630 nm of ligand free perovskite material with the peak 454 nm (perfect blue region) the broad peak arise due to the spherical crystal with range of size 2 to 5 nm and the spherical crystals converted into the tetragonal shape of nanocrystal with size 10 to 70 nm it is confirmed by TEM.

The PL of synthesized inorganic Cs<sub>3</sub>Bi<sub>2</sub>Br<sub>9</sub> perovskite material cover broad wavelength (400 to 560 nm) as shown in Figures 4(c) and (d). Ligand free Cs<sub>3</sub>Bi<sub>2</sub>Br<sub>9</sub> (sample 1) exhibit one peak due to presence of mono-shaped crystal, the peak was blue-shifted compared to sample 2. For sample 2 grown at higher temperature three peak were observed due to formation of various forms of crystal at higher temperature. In the case of sample 1, a sharp narrow peak was observed in UV-Vis spectra at 431 nm and PL was observed at 460 nm as shown in Figure 4(a). But in case of sample 2, in the UV-Vis broad peak was observed at 445 nm and three peaks at 407, 431 and 460 nm were observed as shown in Figure 4(d). The lead and lead free double perovskite bulk have shown difference properties with their nanocrystals. For example CsPbX<sub>3</sub> NCs shows strong quantum confinement effect [23–25]. In Case of double perovskite the band-edge emission of Cs<sub>2</sub>Sb<sub>3</sub>I<sub>9</sub> and Cs<sub>2</sub>Bi<sub>3</sub>I<sub>9</sub> are shows differ with their respective NCs counterpart [26]. When the size of crystal increase (Red side shifted peak) as the absorbance edge of sample 2 is pushed to low energy as a result of decrease the band gap and the PL shows the higher energy peak arise due to indirect band nature. When the PL data fitting the three peaks are 407, 430, 447 respectively, with full range of blue region shown in Figure 4(d) dotted line. In many semiconductors have shown both dopant emission and band-edge emission [27, 28]. At higher temperature the absorbance, a red shift arises with trap states below the first electronic state (on conduction band). Moreover in lead free and lead base

NCs, both band-edge emission and red shifted has been observed in defect-related emission.

### 3.4. Optical Band GAP

Both indirect and direct nature of band gap of bismuth based materials due to exciton recombination process, temperature dependence has been reported using density functional theory (DFT).

The equation for calculating the optical band gap is given below

$$\alpha h\nu = \sqrt{h\nu - E_g}$$

Where  $\alpha$  is the absorption coefficient and  $h\nu$  is the energy of photon with frequency ( $h$ ) Planck constant and frequency ( $\nu$ ) and  $E_g$  is the optical bandgap energy.

Using this equation we can find out the band gap and the nature of direct and indirect band gap can be deduced using the formula.

$$\text{Direct bandgap} = (\alpha h\nu)^2$$

$$\text{Indirect bandgap} = (\alpha h\nu)^{0.5}$$

$$h\nu = \frac{1240.59}{\lambda}$$

Where  $\lambda$  is the wavelength.

Figure 5 shows the Tauc's plot for samples. Both bismuth based samples shows absorbance tails lower energies, which have been shows to indirect band gap [29]. Tauc plot and estimated the optical direct and indirect band gap for samples 1 are 2.78 eV and 2.67 eV respectively. But the optical direct and indirect band gap for samples 2 (higher temperature reaction) are 2.31 eV and 2.55 eV respectively, which are similar to their bulk counterpart. Therefore neither of both samples shows strong quantum confinement effects.

### 3.5. Time-Resolved Photoluminescence

The Tri-exponential function has been used for investigation the size dependent improve the trap state of upper

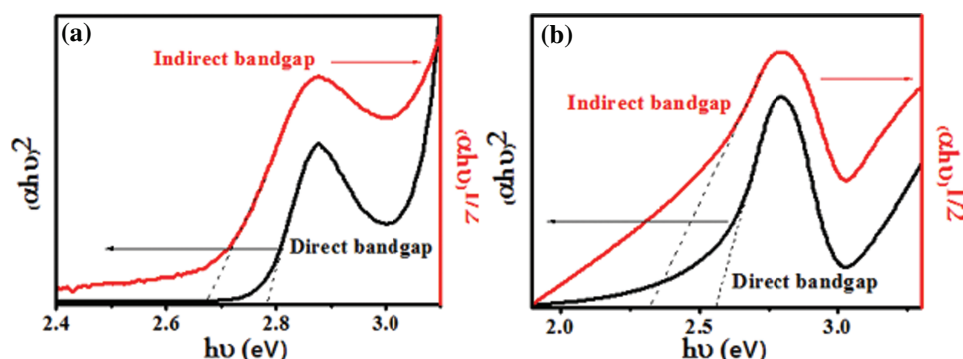
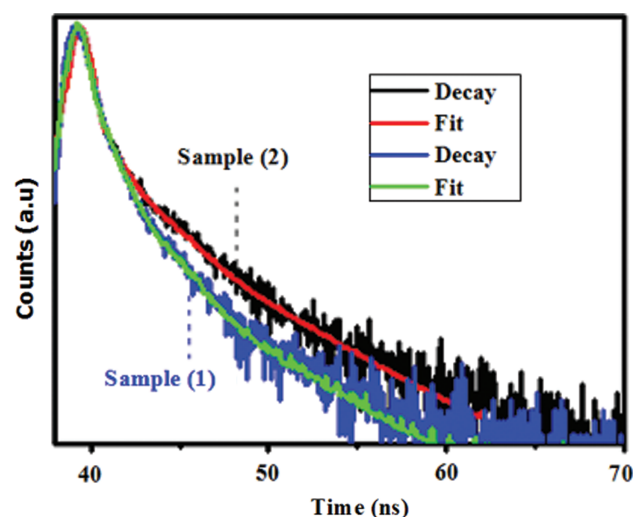


Figure 5. Sample 1 (a) and sample 2 (b). Direct and indirect band gap from Tauc plot.



**Figure 6.** TRPL decay and fit profile sample 1 and 2 emission wavelengths 460 nm (2.69 eV).

band and quantum confinement in Cs<sub>3</sub>Bi<sub>2</sub>Br<sub>9</sub>. Two type of Cs<sub>3</sub>Bi<sub>2</sub>Br<sub>9</sub> with average size of  $3.0 \pm 0.5$  nm and the range size 10 to 70 nm were investigated using TRPL (Fig. 6). All the TRPL decay profiles were fitted by using Tri exponential function with the help of DAS 6 Software.

$$I(t) = \alpha_1 \exp(-t/\tau_1) + \alpha_2 \exp(-t/\tau_2) + \alpha_3 \exp(-t/\tau_3) \quad (1)$$

$$\tau_{\text{avg}} = \frac{\sum \alpha_i \tau_i^2}{\sum \alpha_i \tau_i} \quad (2)$$

Where the Time Constant ( $\tau_1, \tau_2, \tau_3$ ) and exponential function ( $\alpha_1, \alpha_2, \alpha_3$ ) represent decay time and the relative amplitude each component, respectively.

The Time-Resolved photoluminescence (TRPL) measurement on both sample 1 and 2 were carried out using correlated single photo counting (TCSPC) system. The decay were fitted by Tri exponential function with short lived component  $\tau_1$  ( $1.44 \times 10^{-11}$  s), ( $8.87 \times 10^{-11}$  s) a middle component  $\tau_2$  ( $1.274 \times 10^{-9}$  s), ( $1.649 \times 10^{-9}$  s) and final ultra-long lived component (edge state)  $\tau_3$  ( $5.488 \times 10^{-9}$  s), ( $6.164 \times 10^{-9}$  s) respectively.

The results are also shown in Table I, The calculated average life time for Cs<sub>3</sub>Bi<sub>2</sub>Br<sub>9</sub> QDs and NCs were 3.067 ns and 4.761 ns respectively. The major difference in time components between two samples is the ratio of fast and middle component. We know that TRPL is not effective the consecration of liquid sample. The Time-resolved photoluminescence decay of perovskite NCs are

**Table I.** TRPL decay components, relative amplitude, average life time of sample 1 and 2 with  $\chi^2$  (XSQ) value.

Cs <sub>3</sub> Bi <sub>2</sub> Br <sub>9</sub>	$\alpha_1$ %	$\tau_1$ (ns)	$\alpha_2$ %	$\tau_2$ (ns)	$\alpha_3$ %	$\tau_3$ (ns)	$\tau_{\text{avg}}$ (ns)
Sample 1	92.87	0.014	5.83	1.274	1.30	5.488	3.067
Sample 2	64.37	0.088	20.43	1.649	15.20	6.164	4.761

shows much shorter PL lifetime corresponding to the bulk single crystal counterpart because of the stronger overlap between electron-hole wave function in a dimension on confined space and electron-phonon commonly shows band gap behaviour of increasing to temperature [30–32]. The small size of quantum dots make them almost to be defect free, dominating to excitations being more level to radiative recombination. The fast decay component can be naturally attributed to quenching of PL and is affected by particle size. The  $\tau_3$  component can be attributed to edge state associated with decay pathway. The difference in average time for samples 1 and 2 are arises with trap states below the first electronic state and may be excessive trap in material as a result non-radiative decay of excitons exceed the way.

#### 4. CONCLUSION

First time benzoyl Bromide precursor is use for colloidal synthesis of lead free double perovskite nanocrystal of Cs<sub>3</sub>Bi<sub>2</sub>Br<sub>9</sub>. Benzoyl Bromide was worked as a bromide precursor with differ temperature injected it. The Colloidal of Cs<sub>3</sub>Bi<sub>2</sub>Br<sub>9</sub> material with spherical and tetragonal structure as synthesized by using hot injection method. The optical and structural properties of Cs<sub>3</sub>Bi<sub>2</sub>Br<sub>9</sub> have been studied. There are two features in both absorption and emission spectra of Cs<sub>3</sub>Bi<sub>2</sub>Br<sub>9</sub>. The UV-Vis spectrum of Cs<sub>3</sub>Bi<sub>2</sub>Br<sub>9</sub> shows excitonic band gap with direct band gap of sample 1 and 2 are 2.74 and 2.31 eV respectively.

**Acknowledgments:** One of the author Ashish Kumar, acknowledges CSIR for grant of JRF. Sanjay Kumar Swami thanks Department of Science and Technology (DST), New Delhi for Inspire Faculty Award. Authors are grateful to Director, CSIR-NPL for granting permission to publish this result.

#### References and Notes

- Bass, K.K., Estergreen, L., Savory, C.N., Buckeridge, J., Scanlon, D.O., Djurovich, P.I., Bradforth, S.E., Thompson, M.E. and Melot, B.C., **2016**. Vibronic structure in room temperature photoluminescence of the halide perovskite Cs<sub>3</sub>Bi<sub>2</sub>Br<sub>9</sub>. *Inorganic Chemistry*, 56(1), pp.42–45.
- Elseman, A.M., Shalan, A.E., Sajid, S., Rashad, M.M., Hassan, A.M. and Li, M., **2018**. Copper-substituted lead perovskite materials constructed with different halides for working (CH<sub>3</sub>NH<sub>3</sub>)<sub>2</sub>CuX<sub>4</sub>-based perovskite solar cells from experimental and theoretical view. *ACS Applied Materials & Interfaces*, 10(14), pp.11699–11707.
- McClure, E.T., Ball, M.R., Windl, W. and Woodward, P.M., **2016**. Cs<sub>2</sub>AgBiX<sub>6</sub> (X = Br, Cl): New visible light absorbing, lead-free halide perovskite semiconductors. *Chemistry of Materials*, 28(5), pp.1348–1354.
- Slavney, A.H., Hu, T., Lindenberg, A.M. and Karunadasa, H.I., **2016**. A bismuth-halide double perovskite with long carrier recombination lifetime for photovoltaic applications. *Journal of the American Chemical Society*, 138(7), pp.2138–2141.
- Jellicoe, T.C., Richter, J.M., Glass, H.F., Tabachnyk, M., Brady, R., Dutton, S.E. and Böhm, M.L. **2016**. Synthesis and optical properties of lead-free cesium tin halide perovskite nanocrystals. *Journal of the American Chemical Society*, 138(9), pp.2941–2944.

6. McMeekin, D.P., Sadoughi, G., Rehman, W., Eperon, G.E., Saliba, M., Hörlantner, M.T. and Johnston, M.B., **2016**. A mixed-cation lead mixed-halide perovskite absorber for tandem solar cells. *Science*, *351*(6269), pp.151–155.
7. Song, J., Li, J., Li, X., Xu, L., Dong, Y. and Zeng, H., **2015**. Quantum dot light-emitting diodes based on inorganic perovskite cesium lead halides (CsPbX<sub>3</sub>). *Advanced Materials*, *27*(44), pp.7162–7167.
8. Wang, Y., Li, X., Song, J., Xiao, L., Zeng, H. and Sun, H., **2015**. All-inorganic colloidal perovskite quantum dots: A new class of lasing materials with favorable characteristics. *Advanced Materials*, *27*(44), pp.7101–7108.
9. Fu, Y., Zhu, H., Stoumpos, C.C., Ding, Q., Wang, J., Kanatzidis, M.G., Zhu, X. and Jin, S., **2016**. Broad wavelength tunable robust lasing from single-crystal nanowires of cesium lead halide perovskites (CsPbX<sub>3</sub>, X = Cl, Br, I). *ACS Nano*, *10*(8), pp.7963–7972.
10. Wang, Y., Li, X., Song, J., Xiao, L., Zeng, H. and Sun, H., **2015**. All-inorganic colloidal perovskite quantum dots: A new class of lasing materials with favorable characteristics. *Advanced Materials*, *27*(44), pp.7101–7108.
11. Fu, Y., Zhu, H., Stoumpos, C.C., Ding, Q., Wang, J., Kanatzidis, M.G., Zhu, X. and Jin, S., **2016**. Broad wavelength tunable robust lasing from single-crystal nanowires of cesium lead halide perovskites (CsPbX<sub>3</sub>, X = Cl, Br, I). *ACS Nano*, *10*(8), pp.7963–7972.
12. Song, J., Li, J., Li, X., Xu, L., Dong, Y. and Zeng, H., **2015**. Nanocrystals: Quantum dot light-emitting diodes based on inorganic perovskite cesium lead halides (CsPbX<sub>3</sub>). *Advanced Materials*, *27*(44), pp.7161–7161.
13. Leng, M., Chen, Z., Yang, Y., Li, Z., Zeng, K., Li, K., Niu, G., He, Y., Zhou, Q. and Tang, J., **2016**. Lead-Free, blue emitting bismuth halide perovskite quantum dots. *Angewandte Chemie International Edition*, *55*(48), pp.15012–15016.
14. Park, B.W., Philippe, B., Zhang, X., Rensmo, H., Boschloo, G. and Johansson, E.M., **2015**. Bismuth based hybrid perovskites A<sub>3</sub>Bi<sub>2</sub>I<sub>9</sub> (A: Methylammonium or cesium) for solar cell application. *Advanced Materials*, *27*(43), pp.6806–6813.
15. Imran, M., Caligiuri, V., Wang, M., Goldoni, L., Prato, M., Krahne, R., De Trizio, L. and Manna, L., **2018**. Benzoyl halides as alternative precursors for the colloidal synthesis of lead-based halide perovskite nanocrystals. *Journal of the American Chemical Society*, *140*(7), pp.2656–2664.
16. Yang, B., Chen, J., Hong, F., Mao, X., Zheng, K., Yang, S., Li, Y., Pullerits, T., Deng, W. and Han, K., **2017**. Lead-free, air-stable all-inorganic cesium bismuth halide perovskite nanocrystals. *Angewandte Chemie*, *129*(41), pp.12645–12649.
17. Lazarini, F., **1977**. Caesium enneabromodibismuthate (III). *Acta Crystallographica Section B*, *33*(9), pp.2961–2964.
18. Timmermans, C.W.M. and Blasse, G., **1981**. On the luminescence of Cs<sub>3</sub>Bi<sub>2</sub>Br<sub>9</sub> single crystals. *Physica Status Solidi (b)*, *106*(2), pp.647–655.
19. Langevin, M.A., Ritcey, A.M. and Allen, C.N., **2014**. Air-stable near-infrared AgInSe<sub>2</sub> nanocrystals. *ACS Nano*, *8*(4), pp.3476–3482.
20. Timmermans, C.W.M., Cholakh, S.O., Van der Woude, R.L. and Blasse, G., **1983**. Some optical and electrical measurements on Cs<sub>3</sub>Bi<sub>2</sub>Br<sub>9</sub> single crystals. *Physica Status Solidi (b)*, *115*(1), pp.267–271.
21. Miller, O.D., Yablonovitch, E. and Kurtz, S.R., **2012**. Strong internal and external luminescence as solar cells approach the Shockley–Queisser limit. *IEEE Journal of Photovoltaics*, *2*(3), pp.303–311.
22. Yang, B., Chen, J., Hong, F., Mao, X., Zheng, K., Yang, S., Li, Y., Pullerits, T., Deng, W. and Han, K., **2017**. Lead-free, air-stable all-inorganic cesium bismuth halide perovskite nanocrystals. *Angewandte Chemie*, *129*(41), pp.12645–12649.
23. Protesescu, L., Yakunin, S., Bodnarchuk, M.I., Krieg, F., Caputo, R., Hendon, C.H., Yang, R.X., Walsh, A. and Kovalenko, M.V., **2015**. Nanocrystals of cesium lead halide perovskites (CsPbX<sub>3</sub>, X = Cl, Br, and I): Novel optoelectronic materials showing bright emission with wide color gamut. *Nano Letters*, *15*(6), pp.3692–3696.
24. Swarnkar, A., Chulliyil, R., Ravi, V.K., Irfanullah, M., Chowdhury, A. and Nag, A., **2015**. Colloidal CsPbBr<sub>3</sub> perovskite nanocrystals: Luminescence beyond traditional quantum dots. *Angewandte Chemie*, *127*(51), pp.15644–15648.
25. Mondal, N., De, A. and Samanta, A., **2018**. Achieving near-unity photoluminescence efficiency for blue-violet-emitting perovskite nanocrystals. *ACS Energy Letters*, *4*(1), pp.32–39.
26. Pal, J., Manna, S., Mondal, A., Das, S., Adarsh, K.V. and Nag, A., **2017**. Colloidal synthesis and photophysics of M<sub>3</sub>Sb<sub>2</sub>I<sub>9</sub> (M = Cs and Rb) nanocrystals: Lead-free perovskites. *Angewandte Chemie International Edition*, *56*(45), pp.14187–14191.
27. Pradhan, N. and Sarma, D.D., **2011**. Advances in light-emitting doped semiconductor nanocrystals. *The Journal of Physical Chemistry Letters*, *2*(21), pp.2818–2826.
28. Pal, J., Bhunia, A., Chakraborty, S., Manna, S., Das, S., Dewan, A., Datta, S. and Nag, A., **2018**. Synthesis and optical properties of colloidal M<sub>3</sub>Bi<sub>2</sub>I<sub>9</sub> (M = Cs, Rb) perovskite nanocrystals. *The Journal of Physical Chemistry C*, *122*(19), pp.10643–10649.
29. Creutz, S.E., Crites, E.N., De Siena, M.C. and Gamelin, D.R., **2018**. Colloidal nanocrystals of lead-free double-perovskite (elpasolite) semiconductors: Synthesis and anion exchange to access new materials. *Nano Letters*, *18*(2), pp.1118–1123.
30. Hu, F., Zhang, H., Sun, C., Yin, C., Lv, B., Zhang, C., Yu, W.W., Wang, X., Zhang, Y. and Xiao, M., **2015**. Superior optical properties of perovskite nanocrystals as single photon emitters. *ACS nano*, *9*(12), pp.12410–12416.
31. Dohner, E.R., Jaffe, A., Bradshaw, L.R. and Karunadasa, H.I., **2014**. Intrinsic white-light emission from layered hybrid perovskites. *Journal of the American Chemical Society*, *136*(38), pp.13154–13157.
32. Yu, C., Chen, Z., J. Wang, J., Pfenninger, W., Vockic, N., Kenney, J.T. and Shum, K., **2011**. Temperature dependence of the band gap of perovskite semiconductor compound CsSnI<sub>3</sub>. *Journal of Applied Physics*, *110*(6), p.063526.

Received: 27 August 2018. Accepted: 20 March 2019.